Sustainable Energy & Fuels

Ammonia synthesis from nitrogen and water at intermediate temperatures and elevated pressures by using an electrochemical hydrogen-membrane reactor with supported Ru catalysts and phosphate electrolytes.

Journal:	*Sustainable Energy & Fuels*
Manuscript ID	SE-ART-01-2019-000049.R2
Article Type:	Paper
Date Submitted by the Author:	11-Mar-2019
Complete List of Authors:	Imamura, Kanako; Fukuoka University Kubota, Jun; Fukuoka University

Sustainable Energy & Fuels

PAPER

Ammonia synthesis from nitrogen and water at intermediate temperatures and elevated pressures by using an electrochemical hydrogen-membrane reactor with supported Ru catalysts and phosphate electrolytes.

Received 00th January 20xx,
Accepted 00th January 20xx

DOI: 10.1039/x0xx00000x

www.rsc.org/

Kanako Imamura[a] and Jun Kubota*[a]

Electrochemical synthesis of NH_3 from N_2 and H_2O with electrical power is a promising technology to convert redundant electricity to chemical fuel. NH_3 synthesis from N_2 and H_2O using a combination of Cs-promoted Ru catalysts, a Pd-based hydrogen-membrane cathode, a CsH_2PO_4/SiP_2O_7 electrolyte, and a Pt anode was investigated in the temperature range of 200-250°C and pressure range of 0.1-0.7 MPa. A maximum NH_3 formation rate of 12.4 nmol s^{-1} cm^{-2} (759 μg h^{-1} cm^{-2}) was obtained at 250°C and 0.7 MPa using 5 wt%-Ru/Cs^+/MgO (Cs/Ru = 1 mol) for a current density of 30 mA cm^{-2}. The corresponding current efficiency for NH_3 formation was estimated to be 12%, and the remaining part of the current was confirmed to be used for H_2 production. The NH_3 formation rate increased upon increasing the total pressure, following thermodynamic equilibrium. 5 wt%-Ru/Cs^+/CeO_2 (Cs/Ru = 1 atom) was found to yield the highest formation rate of NH_3 at 200-220°C and 0.1 MPa, while Ru/Cs^+/MgO yielded a higher NH_3 formation rate than Ru/Cs^+/CeO_2 under the elevated pressure condition. Because the dissociation of linearly adsorbed molecular N_2 on Ru is known to be the rate-determining step in NH_3 synthesis, infrared spectroscopy was utilized to examine the linearly adsorbed N_2 on the Ru sites at the adsorption equilibrium at 30°C.

Introduction

The utilization of redundant electricity, which is obtained from renewable sources such as solar, wind, and oceanic energies, is a key technology for the establishment of a future energy society.[1-3] Fluctuation and non-uniformity on the earth are essential attributes of such natural energies, which is not ideal for human demands. For instance, some solar power plants on Kyushu island of Japan (Kyushu Electric Power Co. Inc.) were suspended for a few days in Oct 2018 to avoid blackouts due to the redundancy of electricity when there was abundant sunlight.[4] The conversion of such electricity to chemical energy is a key technology to store, transport, and utilize such energy.

Ammonia (NH_3), one of the major artificially synthesized chemicals, which is mainly consumed as fertilizers, is currently produced from N_2 and H_2 obtained from air and fossil resources, respectively.[5-7] NH_3 can be used as a chemical fuel if it is synthesized by renewable energy.[8-12] The largest advantage of NH_3 as an energy carrier is that it can be directly applied to combustion engines[13-17] and high-temperature fuel cells[18-21] as a fuel. The exhaust from NH_3 combustion essentially consists of N_2 and H_2O, which can be safely released to the air. A second advantage of NH_3 is that it can be readily liquefied under slight pressurization (20°C, 0.86 MPa). Thus, the ease of storage as a liquefied fuel and handling as a gas fuel are clear advantages of NH_3. About 150-170 million tons of NH_3 were artificially synthesized and consumed worldwide in 2017.[22,23] Therefore, infrastructure such as storage tanks, carrier ships, carrier vehicles, and pipelines has already been established. A third advantage of NH_3 over other hydrogen carriers such as methylcyclohexane (MCH) and hydrogen absorbing alloys is its high weight percentage of hydrogen (17.8 wt%). The dehydrogenation heat of $\Delta_r H°$ = 31 kJ mol^{-1}-H_2 is much smaller than that for MCH (68 kJ mol^{-1}-H_2).[24] Therefore, NH_3 is an appropriate source even for obtaining H_2. NH_3 is thus suitable as a source of hydrogen. The synthesis of NH_3 from N_2 and H_2O by renewable electricity is referred to as "power-to-ammonia technology" and is a promising strategy for the establishment of a renewable energy society.[25]

With conventional technologies, NH_3 can be produced from N_2 and H_2O using a combination of water electrolysis and the Haber-Bosch process. In water electrolysis under standard conditions, an enthalpy of $\Delta_r H°$ = 286 kJ mol^{-1} is required to split liquid H_2O.[26] The major part of the energy is the Gibbs

[a] Department of Chemical Engineering, Fukuoka University, 8-19-1, Nanakuma, Jonan-ku, Fukuoka 814-0180, Japan
E-mail: jkubota@fukuoka-u.ac.jp

† Footnotes relating to the title and/or authors should appear here.
Electronic Supplementary Information (ESI) available: [details of any supplementary information available should be included here]. See

energy, $\Delta_r G° = 237$ kJ mol^{-1}, which is provided by applied electricity with the theoretical voltage of 1.23 V and flow of 2-electrons per molecule, but not from heat. The remaining part, 49 kJ mol^{-1}, which is corresponding to entropy change, is supplied as heat, so that water electrolysis is theoretically endothermic reaction. On the other hand, the Haber-Bosch process is an exothermic reaction with 31 kJ mol^{-1}-H_2.[5-7,26,27] If the two processes operate independently, the endothermic and exothermic components should be treated separately. Direct NH_3 synthesis from N_2 and H_2O using electricity has a smaller theoretical voltage of 1.17 V with a smaller endothermic heat of 29 kJ mol^{-1}-H_2. According to calculations for water vapour, this reaction releases an exothermic heat of 7 kJ mol^{-1}-H_2. As a simple concept, a combination of exothermic NH_3 synthesis of 31 kJ mol^{-1}-H_2 and endothermic water electrolysis of 49 kJ mol^{-1} at a same temperature in a single reactor results in a thermally balanced process. It should be noted that these energies are values for standard conditions. The thermodynamic parameters are shown in electronic supplementary information (ESI). The theoretical voltage and heat are same whether either N_2 is electrochemically reduced or N_2 is reduced by electrolyzed H_2, if the whole system is in thermal equilibrium. Thus, the development of NH_3 synthesis from N_2 and H_2O using electricity has attracted much interest in the past few years.[25,28-34] Although these endothermic and exothermic energies in the individual elemental parts are much smaller than the main energy input as electricity to the electrochemical reactor, which is derived from the theoretical electrolysis voltage of 1.17 V, thermally balanced chemical reactors should be essentially favorable. Electrochemical devices have the advantage of easy start-and-stop operation, similar to fuel cells, compared to industrial chemical plants such as Haber-Bosch process. The electrochemical devices are generally suitable for small-scale distributed energy systems. The advantages of NH_3 synthesis from N_2 and H_2O by electricity using a single electrochemical devise are that the exothermic and endothermic heats are balanced out and this is a small scale devise suitable to dispersed power systems.

For the reasons mentioned above, there have been many efforts devoted toward the electrochemical synthesis of NH_3.[8,25,28-34] The operating temperature of solid oxide electrolyte systems is typically over 500°C, and the production of NH_3 is strongly limited by thermodynamic equilibrium.[5-7,27] Under such conditions, most NH_3 is spontaneously decomposed to N_2 and H_2, even if it is synthesized electrochemically at an amount over the thermodynamic limitation. The electrochemical synthesis of NH_3 in aqueous or polymer electrolytes below 100°C has been studied by many researchers. Artificial nitrogen fixation under ambient conditions is an dream chemical reaction, as well as artificial photosynthesis; however, it is challenging to obtain a sufficient amount of NH_3 by artificial catalysts in a continuous manner to meet industrial demands. The $N \equiv N$ bond of N_2 is extremely stable and difficult to activate by solid catalysts at ambient temperature conditions. Therefore, considering both thermodynamic limitations and the activation of N_2 molecules, we examined NH_3 synthesis in the temperature range of 200-250°C.

In our previous work, we demonstrated a new type of electrochemical system for NH_3 synthesis from N_2 and H_2O using electricity.[35,36] The basic concept is illustrated in Fig. 1. The cell consists of a Ru catalyst, a hydrogen-permeable Pd-Ag membrane cathode, a phosphate-based electrolyte, and a Pt anode operated in the temperature range of 200-250°C. Variety of protonic ionomers such as oxides,[37-40] oxyacid salts,[41] and ion-exchange polymers[42] cover over ambient and intermediate temperature range up to ~500°C with appropriate conductivities, which have been examined for electrochemical NH_3 synthesis. Among them, CsH_2PO_4-based electrolytes has been used in the present system. The use of the hydrogen-permeable Pd-Ag membrane enables the isolation of the NH_3 product from the acidic and protonic phosphate-based electrolyte by preventing the absorption of NH_3 into the electrolyte and the humidification of the Ru catalyst. The application of hydrogen-permeable membranes to electrochemical cells has been previously reported for fuel cells.[43-46] NH_3 synthesis in the temperature range of 200~250°C, which is much lower than that for the Haber-Bosch process (400~500°C), is one of the primary challenges in NH_3 catalysis. We examined only Cs^+-promoted Ru/MgO catalysts as a rudimentary electrochemical system in our previous work. The NH_3 synthesis rate of 0.90 nmol s^{-1} cm^{-2} with a current efficiency of 2.6% was obtained at 250°C and 10 mA cm^{-2}, thus demonstrating the newly designed electrochemical system. However, elevated pressure conditions and a variety of catalysts were not investigated.

Ru catalysts are known to have significant NH_3 synthesis activity, especially near atmospheric pressure conditions, when Ru particles are influenced by electronegative promoters and supports such as alkali metal compounds,[5-7,47,48] rare-earth materials,[49,50] and electrides.[51,52] In NH_3 synthesis, the dissociation of adsorbed N_2 on Ru sites is known to be the rate-determining step.[5-7,47,48] The nature of the adsorbed N_2 on Ru sites provides important information on the activity of the catalysts. The vibrational frequencies of the $N \equiv N$ bond of linearly-adsorbed N_2 on metallic Ru sites has been reported to

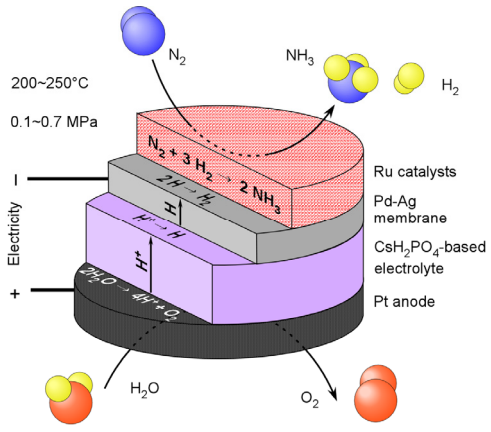

Fig. 1 Concept of hydrogen-membrane electrochemical reactor for NH_3 synthesis.

be an indication of the weakening of the N≡N bond on Ru catalysts.[47-53] The infrared spectra of adsorbed N_2 on Ru sites were examined in this paper.

In this work, we examined NH_3 synthesis from N_2 and H_2O using electrical power with Ru/Cs^+/MgO, Ru-Cs^+/CeO_2 and Ru/Cs^+/CeO_2 catalysts at elevated pressure of 0.7 MPa. The selectivity of NH_3 production against H_2 production was investigated both thermodynamically and kinetically. The properties of adsorbed N_2 on Ru sites were examined using infrared spectroscopy.

Experimental

Materials preparation

The experimental setup and procedures were similar to those in our previous reports.[35,36]

Ru catalysts of 5 wt%-Ru/Cs^+/MgO and 5 wt%-Ru/Cs^+/CeO_2 (Cs/Ru = 1 mol) were synthesized as follows. MgO (Reference catalyst of Catalysis Society of Japan, JRC-MGO-4 500A provided by Ube Material Industries) with Brunauer-Emmett-Teller (BET) specific surface area of 28-38 $m^2\ g^{-1}$ and CeO_2 (Reference catalyst of Catalysis Society of Japan, JRC-CEO-5 provided by Daiichi Kigenso Kagaku Kogyo) with BET specific surface area of 92 $m^2\ g^{-1}$ were calcined at 500°C in air to remove adsorbed impurities. The catalysts were immersed in a tetrahydrofuran solution of $Ru_3(CO)_{12}$ (Tanaka Kikinzoku Kogyo) at room temperature for several hours with stirring. The slurries were evaporated under reduced pressure below 50°C to avoid decomposition of $Ru_3(CO)_{12}$. The obtained powders were treated at 300°C in vacuum to desorb the carbonyl groups. For addition of the Cs^+ promoter, Ru/MgO and Ru/CeO_2 were immersed in an aqueous solution of $CsNO_3$ (Fujifilm-Wako) for a few hours followed by drying. Finally, the catalysts were treated under H_2 flow at 300°C. The catalyst powder was formed into granules using a hydraulic press, and 600–800 μm granules were sorted by sieving. The specific chemical state of Cs^+ was difficult to establish, since it could be present as CsOH, Cs_2O, Cs_2CO_3, etc. under changing atmospheric conditions, and thus we express it as Cs^+.

A 100 μm thick Pd–Ag foil (Nilaco Co.) containing 25% Ag on a molar basis was cut to form a disk of 24 mm diameter.

CsH_2PO_4 was obtained by the mixing of appropriate concentrations and amounts of aqueous solutions of Cs_2CO_3 (Fujifilm-Wako) and H_3PO_4 (Fujifilm-Wako). The mixed aqueous solution was dried at 120°C to obtain CsH_2PO_4. SiP_2O_7 was obtained by the kneading of H_3PO_4 and SiO_2 (Sigma-Aldrich). The viscous slurry was calcined at 200°C for 3 h and 500°C for 3 h. CsH_2PO_4 and SiP_2O_7 were mixed with a mortar in a 1:2 molar ratio. The CsH_2PO_4/SiP_2O_7 powders were pressed into a disk of 20 mm diameter and 2 mm thickness by a hydraulic machine.

Pt paste (Tanaka Kikinzoku Kogyo K.K.) was spread on carbon paper (Toray, TGP-H-120H) with a diameter of 20 mm at a density of ca. 3 mg-Pt cm^{-2}, and then dried at 300°C.

The Pd-Ag foil, CsH_2PO_4/SiP_2O_7 disk and Pt-coated carbon paper were then placed on top of each other and hot-pressed at 3 MPa and 220°C by a hydraulic machine.

Materials characterization

Morphological observations were carried out using a JEOL JEM-2100F transmission electron microscope (TEM) at Kyushu University. The crystal structures of CsH_2PO_4 and SiP_2O_7 were analysed by X-ray diffraction (XRD, Shimadzu, XRD-6100).

For infrared spectroscopic measurements, the detailed experimental setup is shown in ESI. Briefly, 100 mg of sample catalysts were pressed into disks of 20 mm diameter by a hydraulic press. The sample disk was placed in an infrared cell made of quartz glass which was equipped with two CaF_2 windows. The cell was connected to a closed circulation and vacuum system made of glass which was evacuated by a mechanical rotary pump with a liquid nitrogen-cooled trap.

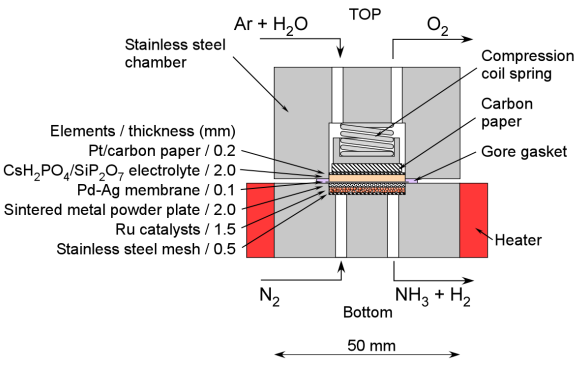

Fig. 2 Cross-sectional view of electrochemical hydrogen-membrane reactor on a realistic scale. The thicknesses of the elements of the membrane assembly are shown in the figure. The top and bottom vessels were tightened together by screws with an insulating layer.

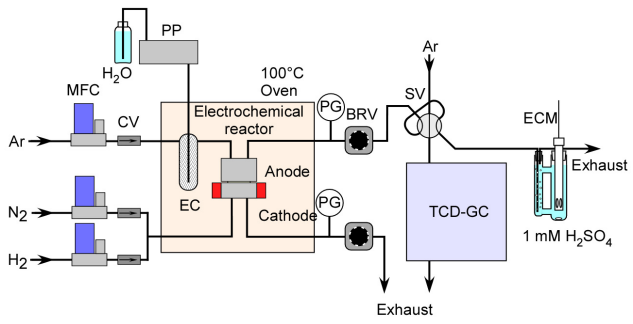

Fig. 3 Illustration of gas system. The abbreviations are as follows: mass flow controller (MFC), check valve (CV), plunger pump (PP), evaporation chamber (EC), pressure gauge (PG), back-pressure regulating valve (BPR), 6-way sampling valve (SV), gas chromatograph with thermal conductivity detector (TCD-GC), and electroconductivity meter (ECM).

Hydrogen-membrane electrochemical reactor

The above materials were placed in a stainless-steel chamber. An illustration of the reactor is shown in Fig. 2. The chamber was made of stainless steel (SUS304) and could hold a hydrogen-membrane/electrolyte/electrode assembly with an effective diameter of 20 mm. The thickness of the catalyst layer was ca. 1.5 mm and the amounts of 5 wt%-Ru/Cs^+/MgO and 5 wt%-Ru/Cs^+/CeO_2 were ca. 130 and 260 mg cm^{-2}, respectively, due to the difference in densities of the support materials.

There were two beneficial changes in the reactor from our previous works.[35,36] First, a sintered metal powder plate of stainless steel with a thickness of 1 mm and a 100 μm pore size was placed between the Pd–Ag foil and catalyst layer. Thus, the Ru catalysts had little contact with the surface of the Pd–Ag foil. The presence of this sintered metal powder plate could keep the Pd–Ag foil flat without deformation after charging of hydrogen in the Pd–Ag foil during operation. Second, the CsH_2PO_4/SiP_2O_7 disk and Pt-coated carbon paper were mechanically pressed into the Pd–Ag foil using a coil spring. Previously, only carbon felt was packed in the excess space. It was found that the mechanical strength was important for maintaining the stacking structure without any gaps and hollows at the interfaces. In our previous paper, the reactor was stably operated at a current density lower than 3.2 mA cm^{-2}, but this could be increased three-fold in the present work.

Gas flow system

The gas system is displayed in Fig. 3. The gas flows on the cathode and anode sides were controlled by mass flow controllers. N_2 and Ar gases were flowed in the cathode and anode side, respectively. For pretreatment, a total N_2+$3H_2$ flow of 28 cm^3_{STP} min^{-1} was introduced to the cathode side to reduce the Ru catalysts. H_2 was connected to the cathode side. The STP value indicates the volume converted to the standard-temperature-pressure (STP) condition of 0°C and 101 kPa. Liquid H_2O was introduced into an evaporation chamber by a plunger pump (Shimazu, LC-10AD). The NH_3 electrochemical reactor and evaporation chamber were placed in an oven to avoid condensing H_2O in the tubing. The exhaust lines from the reactor were equipped with back-pressure regulating valves to pressurize the reactor. The exhaust gas from the cathode side was introduced in 25 mL of 1 mM H_2SO_4 using sintered glass beads to obtain small bubbles. The electroconductivity of this solution was continuously monitored to estimate the amount of NH_3. This exhaust gas could be sampled by a gas chromatograph with a thermal conductivity detector (GL Sciences, GC-3200) to estimate the concentration of H_2.

Results and discussion

Rate of NH_3 formation depending on temperature

The amount of synthesized NH_3, as estimated from the change in electroconductivity of 1 mM H_2SO_4 which absorbed the exhaust of the cathode gas, increased linearly with elapsed time in all cases as shown in our previous papers.[35,36] Thus, the rate of NH_3 formation could be estimated from the slope against time. It should be noted that no NH_3 was detected without Ru catalysts, indicating that NH_3 was not formed from catalytic reaction over the Pd-Ag membrane or decomposition of cell materials such as sealing components or contaminations of inner wall. Although there are many reports for electrochemical synthesis of NH_3 using Pd and Pd-Ag electrode around 500°C as summarized in a liturture,[29] the present Pd-Ag membrane surface was found to be inactive for the NH_3 formation at ~250°C. The rate of NH_3 formation using the electrochemical hydrogen-membrane reactor with a current density of 3.2 mA cm^{-2}, a cathode gas of N_2 of 1 cm^3_{STP} min^{-1}, and an anode gas of Ar of 10 cm^3_{STP} min^{-1} with H_2O of 4 μL-liquid min^{-1} at several temperatures over the range 200-250°C was examined for 5 wt%-Ru/Cs^+/CeO_2 (Cs/Ru = 1 mol), 5 wt%-Ru/Cs^+/MgO (Cs/Ru = 1 mol), and 5 wt%-Ru/CeO_2, and the results are shown in Arrhenius plots in Fig. 4. The thermodynamic limitation of the chemical equilibrium between N_2+H_2 and NH_3, where partial pressures of N_2 and H_2 were estimated from the flow rate of N_2 and current density, respectively, is shown as a dashed line. The physical parameters for the estimation of equilibrium are reported in our previous paper[36], which are referred from a textbook in chemical engineering.[27] The parameters of $\Delta_r G°$, $\Delta_r H°$, and specific heat, C_p are also shown in ESI.[26,27] The partial pressure of H_2 corresponding to the formation of H_2 by 3.2 mA cm^{-2} and that of N_2 corresponding to 1 cm^3_{STP} min^{-1} were used with the

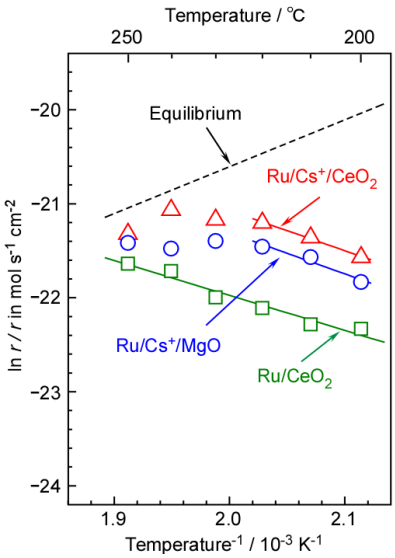

Fig. 4 Arrhenius plots of rate of NH_3 formation for the electrochemical synthesis at a current density of 3.2 mA cm^{-2} and ambient pressure using 5 wt%-Ru/Cs^+/CeO_2 (Cs/Ru = 1 mol), 5 wt%-Ru/Cs^+/MgO (Cs/Ru = 1 mol), and 5 wt%-Ru/CeO_2. The electrochemical hydrogen-membrane reactor was operated with cathode gas of N_2 of 1 cm^3_{STP} min^{-1}, and anode gas of Ar of 10 cm^3_{STP} min^{-1}, with H_2O of 4 μL-liquid min^{-1}.

total pressure of 0.1 MPa for the calculation.

$Ru/Cs^+/CeO_2$ showed the highest rate of NH_3 formation among these catalysts. It should be noted that the weight of $Ru/Cs^+/CeO_2$ (260 mg cm^{-2}) was almost twice that of $Ru/Cs^+/MgO$ (130 mg cm^{-2}) due to the difference in densities. Thus, the specific catalytic activity of $Ru/Cs^+/CeO_2$ per weight was considered to be comparable to that of $Ru/Cs^+/MgO$. Non-promoted Ru/CeO_2 showed the lowest rate of NH_3 formation. In the case of $Ru/Cs^+/CeO_2$ and $Ru/Cs^+/MgO$, the rate of NH_3 formation was close to that estimated from the chemical equilibrium in the range of 240-250°C, indicating that the rate of NH_3 formation was critically limited by the chemical equilibrium. In other words, under thermodynamically favourable conditions such as low temperatures and high pressures, the present electrochemical hydrogen-membrane reactor was expected to generate a greater amount of NH_3. In another aspect, the NH_3 formation close to the chemical equilibrium is due to the use of excess amount of Ru catalysts against the production of electrolyzed H_2. The H_2 production for 3.2 mA cm^{-2} can be converted to 0.071 cm^3_{STP} min^{-1}, so that the residence time of H_2 was remarkably longer than that for conventional NH_3 synthesis from N_2 and H_2. Therefore, even at remarkably lower temperature at 250°C than the Haber-Bosch process, the NH_3 formation was close to thermodynamic limitation. In the case of Ru/CeO_2, the rate of NH_3 formation was clearly lower than the thermodynamic limitation, since there was less catalytic activity.

The apparent activation energies for $Ru/Cs^+/CeO_2$, $Ru/Cs^+/MgO$, and Ru/CeO_2 were estimated from these plots as 36, 31, and 36 kJ mol^{-1}, respectively. It is known that Ru catalysts have apparent activation energies for NH_3 synthesis in the range of 80-150 kJ mol^{-1}, and the apparent activation energies for the present electrochemical hydrogen-membrane reactor were clearly smaller than those. There was no significant difference in the apparent activation energies among these catalysts. We considered that the small apparent activation energy in the present system was due to the low partial pressure of H_2 in the catalyst layer. The H_2 production for 3.2 mA cm^{-2} can be converted to 17 nmol s^{-1} cm^{-2}, as divided by the Faraday constant, while the N_2 flow of 1 cm^3_{STP} min^{-1} corresponds to 240 nmol s^{-1} cm^{-2}. The H_2/N_2 ratio was thus 0.071, which is 42 times smaller than the stoichiometry of 3. Ru catalysts have been generally known to be poisoned by the presence of H_2, i.e., hydrogen poisoning, whereby the presence of H_2 strongly suppresses the activation of N_2 molecules on the Ru sites, which is the rate-determining step in NH_3 synthesis.[5-7,47] The small H_2 partial pressure in the present electrochemical hydrogen-membrane reactor might be due to the small partial pressure of H_2.

Some typical values of rates of NH_3 and H_2 formation and their current efficiencies are listed in Table 1. The current efficiency can be expressed as follows.

$$CE_{NH3} = \frac{3 \times r_{NH3} \times 96485}{j} \times 100$$

$$CE_{H2} = \frac{2 \times r_{H2} \times 96485}{j} \times 100$$

where CE_{NH3} and CE_{H2} are the current efficiencies for NH_3 and H_2 formation in %, respectively, and r_{NH3} and r_{H2} are the rates of NH_3 and H_2 formations in mol s^{-1} cm^{-2}, respectively. The variable j expresses the current density in A cm^{-2}, and 96485 is the Faraday constant in C mol^{-1}. The attainment of equilibrium was also estimated from the ratio of the rate of NH_3 formation against the theoretical thermodynamic equilibrium. The current efficiency of NH_3 is equivalent to the conversion of H_2 to NH_3 in the catalyst layer in the case of the present electrochemical hydrogen-membrane reactor. The sum of CE_{NH3} and CE_{H2} was almost equal to 100%, indicating the current was used for either NH_3 or H_2 formation. The small deviation from 100% was due

Table 1 Rates of NH_3 and H_2 formation, current efficiencies, and attainment of equilibrium (AE) for NH_3 synthesis using the electrochemical hydrogen-membrane reactor at 3.2 mA cm^{-2} and ambient pressure.

Catalyst	Temp.	Rate		Efficiency		AE
		NH_3	H_2	NH_3	H_2	
	˚C	nmol s^{-1} cm^{-2}		%		%
$Ru/Cs^+/CeO_2$	250	0.55	15.7	5.0	95	77
	200	0.43	15.1	3.9	91	22
Ru/CeO_2	250	0.40	16.4	3.6	99	56
	200	0.20	15.2	1.8	92	10
$Ru/Cs^+/MgO$	250	0.50	14.1	4.5	85	70
	200	0.33	11.6	3.0	70	17

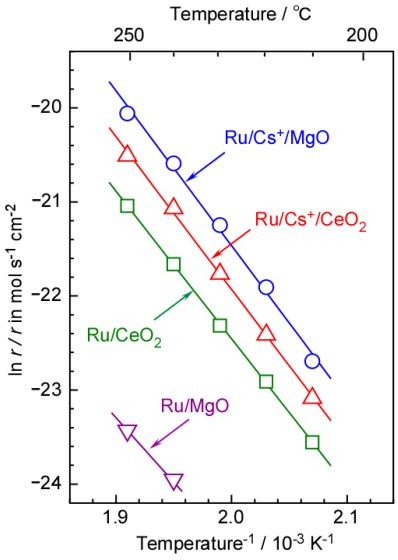

Fig. 5 Arrhenius plots of rate of NH_3 formation from mixture gas of N_2 + 3 H_2 at ambient pressure for 5 wt%-$Ru/Cs^+/CeO_2$ (Cs/Ru = 1 mol), 5 wt%-$Ru/Cs^+/MgO$ (Cs/Ru = 1 mol), 5 wt%-Ru/CeO_2, and 5 wt%-Ru/CeO_2. The flows of N_2 and H_2 were supplied at 7 and 21 cm^3_{STP} min^{-1}, respectively.

to experimental error in gas leakage from the reactor to outside, and cross leakage of H_2 or O_2 through the electrolyte. This deviation was remarkable at lower temperature. As shown in the following section, this deviation became larger for elevated pressure condition. From these facts, leakage through the electrolyte (holes or cracks) or leakage through the sealing materials was considered to be main origin of this deviation. The electrolyte and sealing materials were speculated to soften at higher temperature resulting in the suppression of leakage. The accuracy of the gas chromatograph was speculated to be in a few percent, which was considered to be smaller effect in this deviation. At 250°C, the attainment of equilibrium was reached at 77% for Ru/Cs^+/CeO_2 and the rate of NH_3 formation was found to be mostly limited by the equilibrium.

In the present electrochemical hydrogen-membrane reactor, NH_3 can be produced from the flow of the N_2+3H_2 mixture without electrolysis. The rates of NH_3 formation at the flows of N_2 and H_2 of 7.0 and 21 cm^3_{STP} min^{-1} at 200-250°C were confirmed as shown in Fig. 5. The reactor is completely same to that for the electrochemical synthesis of NH_3, but the voltage was not supplied and the N_2+3H_2 mixture was flowed in cathode side instead of pure N_2. The flow of the N_2+3H_2 mixture was incomparably higher than that obtained by electrolysis. Thus, the equilibrium limit was much higher than the rates of NH_3 formation, which was out of range in Fig. 5. The NH_3 synthesis rates from the N_2+3H_2 mixture were in the order of Ru/Cs^+/MgO, Ru/Cs^+/CeO_2, Ru/CeO_2, and Ru/MgO. Ru/MgO was significantly less active, and thus it is not shown in Fig. 4. The apparent activation energies were estimated as 131, 129, and 125 kJ mol^{-1} for Ru/Cs^+/MgO, Ru/Cs^+/CeO_2, and Ru/CeO_2, respectively, and these values were four times higher than those for the electrolysis shown in Fig. 4. The apparent activation energies for Ru/MgO could not be estimated due to the small rate of NH_3 formation below 240°C, but was similar to the others. In this way, the electrochemical hydrogen-membrane reactor was found to have a characteristic temperature dependence in the rate of NH_3 formation.

The difference in the apparent activation energy between electrochemical NH_3 synthesis from N_2 and H_2O and catalytic NH_3 synthesis from N_2 and H_2 were not found to be dependent on the catalysts or the kinds of supports or presence of promoters of the alkali metal compounds. This means these properties are essential for the electrochemical hydrogen-membrane reactor and independent from the nature of the catalysts.

Rate of NH_3 formation depending on N_2 flow

As described in our previous paper, the dependence of the rate of NH_3 formation on the flow rate of N_2 in the cathode gas provides essential information on the kinetics of NH_3 formation using the electrochemical hydrogen-membrane reactor. The dependence of the rate of NH_3 formation on the flow rate was examined for 5 wt%-Ru/Cs^+/CeO_2 (Cs/Ru = 1 mol), 5 wt%-Ru/Cs^+/MgO (Cs/Ru = 1 mol), and 5 wt%-Ru/CeO_2 at 250°C and ambient pressure, as shown in Fig. 6.

For all three Ru catalysts, the maximum rate of NH_3 formation was obtained for a N_2 flow rate around 0.5-1 cm^3_{STP} min^{-1}. Because the rate of NH_3 formation at 250°C is limited by the thermodynamic equilibrium as shown in Fig. 4, the increase in the rate of NH_3 formation from 10 to 1 cm^3_{STP} min^{-1} of N_2 flow was reasonably understood. The decrease of the N_2 flow led to a H_2/N_2 ratio close to the stoichiometric value of 3, which increased the limit of the thermodynamic equilibrium. The thermodynamic limitation dependence on the H_2/N_2 ratio was shown in our previous paper and a H_2/N_2 ratio of 3 gives, theoretically, the highest NH_3 formation.

At 1 cm^3_{STP} min^{-1} of N_2 flow, the H_2/N_2 ratio was 0.071, 42 times smaller than the stoichiometric value of 3. The thermodynamic equilibrium limit of NH_3 formation depending on the H_2/N_2 ratio was shown in our previous paper.[36] It was expected theoretically that the decrease of the N_2 flow would still cause an increase in the rate of NH_3 formation. However, the rate of NH_3 formation decreased with decreasing N_2 flow below 0.5-1 cm^3_{STP} min^{-1}. In our previous paper, we proposed that the decrease in the rate of NH_3 formation with decreasing N_2 flow was due to increasing H_2 content resulting in hydrogen poisoning. For Ru catalysts, the reaction order of rates of NH_3 synthesis for partial pressure of H_2 is typically a negative number even H_2 is one of reactants, and this nature is called hydrogen poisoning.[5,47] The degree of hydrogen poisoning had been expected to depend on the type of Ru catalysts. However, there was no significant difference in the decrease in the rate of NH_3 formation with decreasing N_2 flow for these three catalysts. The fact that the decrease in the rate of NH_3 formation with decreasing N_2 flow below 1 cm^3_{STP} min^{-1} did not follow the

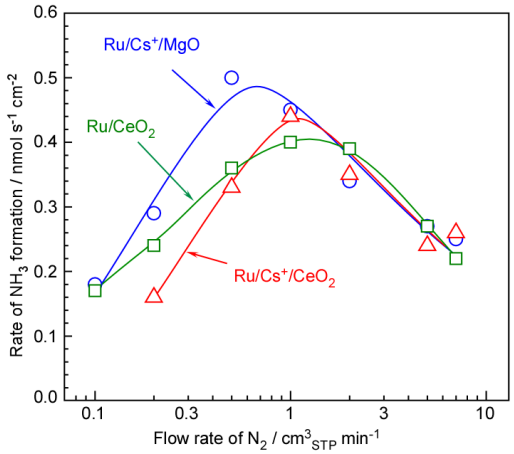

Fig. 6 Dependence of rate of NH_3 formation on the N_2 flow rate for the electrochemical synthesis at a current density of 3.2 mA cm^{-2} and ambient pressure using 5 wt%-Ru/Cs^+/CeO_2 (Cs/Ru = 1 mol), 5 wt%-Ru/Cs^+/MgO (Cs/Ru = 1 mol), and 5 wt%-Ru/CeO_2. The electrochemical hydrogen-membrane reactor was operated at 250 ˚C with cathode gas of N_2 of stated flow rates, and anode gas of Ar of 10 cm^3_{STP} min^{-1}, with H_2O of 4 μL-liquid min^{-1}.

thermodynamic equilibrium limit indicated that these catalysts had poor activity under H_2-rich conditions.

Rate of NH_3 formation at elevated pressure

As described above, the rate of NH_3 formation was limited by the thermodynamic equilibrium. To increase the rate of NH_3 formation, the electrochemical hydrogen-membrane reactor was operated at elevated pressure. Fig. 7 shows the rate of NH_3 formation upon elevating pressure. Note that the pressures of the cathode and anode sides were independently regulated by the respective backpressure valves, but both pressures were controlled such that they were balanced at the same pressure. The pressure is expressed as an absolute pressure, e.g., 0.1 MPa is ambient pressure.

With increasing pressure, the rate of NH_3 formation for $Ru/Cs^+/MgO$ increased, following the thermodynamic equilibrium limit. However, the increase in the rate of NH_3 formation with increasing pressure was not significant for $Ru/Cs^+/CeO_2$ or Ru/CeO_2. Under the present condition, $Ru/Cs^+/MgO$ had the best activity. It has been known that $Ru/Cs^+/MgO$ does not increase the rate of NH_3 formation at higher pressures due to hydrogen poisoning. In some cases, Ru catalysts supported by rare earth oxides show higher activity in the high-pressure region since they are less prone to hydrogen poisoning. In the present case, the H_2/N_2 ratio was kept at 0.07 to obtain the highest rate of NH_3 formation, and the small hydrogen content was considered to result in the enhanced rate of NH_3 formation at high pressure for $Ru/Cs^+/MgO$. $Ru/Cs^+/CeO_2$ was found to have a higher rate of NH_3 formation than $Ru/Cs^+/MgO$ as shown in Fig. 4, but this catalyst was not suitable for the elevated pressure conditions.

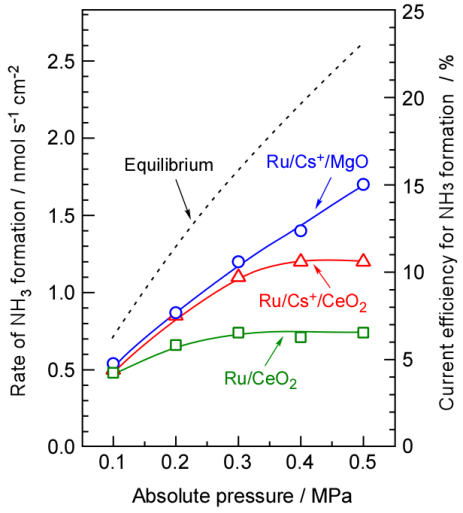

Fig. 7 Rate of NH_3 formation with elevated pressure at a current density of 3.2 mA cm^{-2} using 5 wt%-$Ru/Cs^+/CeO_2$ (Cs/Ru = 1 mol), 5 wt%-$Ru/Cs^+/MgO$ (Cs/Ru = 1 mol), and 5 wt%-Ru/CeO_2. The current efficiency for NH_3 formation is shown in the vertical scale on the right-hand side. The electrochemical hydrogen-membrane reactor was operated at 250 ˚C with cathode gas of N_2 of 1 cm^3_{STP} min^{-1}, and anode gas of Ar of 10 cm^3_{STP} min^{-1}, with H_2O of 4 μL-liquid min^{-1}.

Table 2 Rates of NH_3 and H_2 formation, current efficiencies, and attainment of equilibrium (AE) for NH_3 synthesis at 250 ˚C using the electrochemical hydrogen-membrane reactor at 3.2 mA cm^{-2} and elevated pressure. These data were obtained from Fig. 7.

Catalyst	Pressure	Rate		Efficiency		AE
		NH_3	H_2	NH_3	H_2	
	MPa	nmol s^{-1} cm^{-2}		%		%
$Ru/Cs^+/CeO_2$	0.1	0.50	15.2	4.5	92	71
	0.5	1.2	10.1	12	61	46
Ru/CeO_2	0.1	0.48	16.2	4.3	97	61
	0.5	0.74	14.6	6.7	89	28
$Ru/Cs^+/MgO$	0.1	0.54	16.6	4.9	95	77
	0.5	1.7	11.9	15	72	65

Some typical values of rates of NH_3 and H_2 formation and their current efficiencies with elevated pressure are listed in Table 2. For $Ru/Cs^+/MgO$ at 0.5 MPa, the current efficiency for NH_3 formation was 15%, and the attainment of equilibrium was 65%. The current efficiency increased with increasing pressure as supported by the thermodynamic equilibrium. The attainment of equilibrium was, however, slightly decreased with increasing pressure, indicating that the catalytic activity became insufficient in the higher-pressure region. However, Fig. 7 and Table 2 clearly indicate the possibility of NH_3 synthesis with higher efficiency when the reactor is operated at higher pressure. It should be noted that the total of the current efficiencies of NH_3 and H_2 was significantly smaller than 100% at higher pressure. It was possible that gas leakage from the reactor to outside, and cross leakage of H_2 or O_2 through the electrolyte, were increased at high pressure.

Rate of NH_3 formation at higher current density

Our previous paper showed that the cell voltage of the present electrochemical hydrogen-membrane reactor obviously increased after 10 h under the constant-current operation at 10 mA cm^{-2}. As mentioned in the experimental section, the reactor in this work was modified to obtain a tightened membrane-electrolyte-electrode assembly by pressurization. The generation of clearance gaps at the interface between the hydrogen-membrane and electrolyte was speculated to be the reason for the degradation, and the appropriate pressurization was found to improve the stability. The practical lifetime of the reactor was remarkably prolonged in the present work. The time profiles of the cell voltage for various current densities are shown in Fig. 8. At 30 mA cm^{-2}, the cell voltage increased after several hours due to the degradation, while the cell voltage was stable below 20 mA cm^{-2} for 20 h. Therefore, the NH_3 synthesis in the region from 3.2 to 30 mA cm^{-2} was examined next.

Fig. 9 shows the rates of NH_3 formation and their current efficiencies at 0.7 MPa with increasing current density. With increasing current density, the rate of NH_3 formation monotonically increased, and a rate of NH_3 formation of

12.4 nmol s^{-1} cm^{-2} with a current efficiency of 12% was obtained at 30 mA cm^{-2}. The rate of 12.4 nmol s^{-1} cm^{-2} can be converted to 44.6 μmol h^{-1} cm^{-2} and 759 μg h^{-1} cm^{-2} in other units. At that time, the attainment of equilibrium was estimated as 41%, which was smaller than that at 3.2 mA cm^{-2}. The current efficiency for NH_3 formation decreased with increasing current density. From these observations, it was concluded that the catalysts in the present electrochemical hydrogen-membrane reactor had sufficient activity to almost achieve thermodynamic equilibrium in the lower current density region, especially at lower pressure. However, with increasing current density and pressure, where the rate of NH_3 formation increases, the activity of the catalysts becomes insufficient.

It should be emphasized that in this work, it was considered that the obtained rates of NH_3 formation followed the behaviour of thermodynamic equilibrium. Thus, the detection and analysis of NH_3 in this work should be accurate. Recently, many studies have been performed on the electrochemical synthesis of NH_3 especially at low temperature, and the difficulty of making accurate measurements of synthesized NH_3 is a point of contention.[33] For measurements of small amounts of NH_3, the suppression effect of ambient NH_3 and verification using isotopically labelled nitrogen ($^{15}N_2$) have been strongly suggested for absolute measurements.[33] However, in the present work, the maximum rate of NH_3 formation is 12.4 nmol s^{-1} cm^{-2} (44.6 μmol h^{-1} cm^{-2}), which is 140 μmol h^{-1} for the total output of the present reactor with the area of 3.14 cm^2. For example, the typical rates of NH_3 formation for modern types of NH_3 catalysts have been reported as 13.4 mmol h^{-1} g^{-1} (0.1 MPa, 350°C)[49] for $Ru/La_{0.5}Ce_{0.5}O_{1.75}$ and 2.12 mmol h^{-1} g^{-1} (0.1 MPa, 400°C)[51] for Ru/C12A7:e^-. Therefore, the amount of NH_3 formation in this work is similar to that for typical catalytic NH_3 synthesis from N_2+3H_2 with 0.1 g of catalysts at 0.1 MPa, confirming that there is no serious problem with the detection and measurement of NH_3.

Photographs of the present reactor and for the confirmation of NH_3 formation are shown in Fig. 10. The exhaust gas from the cathode side of the electrochemical hydrogen-membrane reactor (Fig. 10A) was bubbled into pure water with a drop of phenolphthalein ethanol solution as a pH indicator (Fig. 10B). The water with phenolphthalein initially had no colour, but changed to fuchsia within a few minutes as shown in Fig. 10B. This was evidence that the neutralization of 1 mM H_2SO_4 by synthesized NH_3 as monitored with an electroconductivity meter was suitable for the estimation of the amount of NH_3.

Further discussion on the NH_3 synthesis in the present reactor

It should be noted that N_2 molecules are catalytically activated on Ru sites without any application of an electrode potential in the present electrochemical hydrogen-membrane reactor. This means that the N_2 molecules are not electrochemically reduced but reduced by H_2 or H produced by electrolysis of water. Only protons are reduced electrochemically and these are supplied to the Ru sites through the gas phase as H_2 and/or migration on the catalytic surfaces. In a precise sense, because N_2 molecules are not electrochemically reduced directly on the electrode, the electrochemical hydrogen-membrane reactor does not perform direct electrochemical synthesis of NH_3. The overall reaction scheme of this system is:

$$N_2 + 3\ H_2O \rightarrow 2\ NH_3 + 3/2\ O_2$$

The overall endo/exothermic heat and change in Gibbs energy,

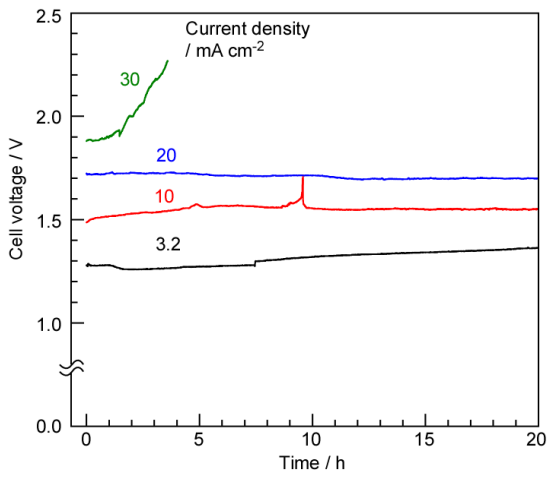

Fig. 8 Time courses of cell voltage for the operation with constant current at various current densities. The electrochemical hydrogen-membrane reactor was operated with 5 wt%-Ru/Cs^+/MgO (Cs/Ru = 1 mol) at 250 ˚C and 0.1 MPa with cathode gas of N_2 of 1 cm^3_{STP} min^{-1}, and anode gas of Ar of 10 cm^3_{STP} min^{-1}, with H_2O of 4 μL-liquid min^{-1}.

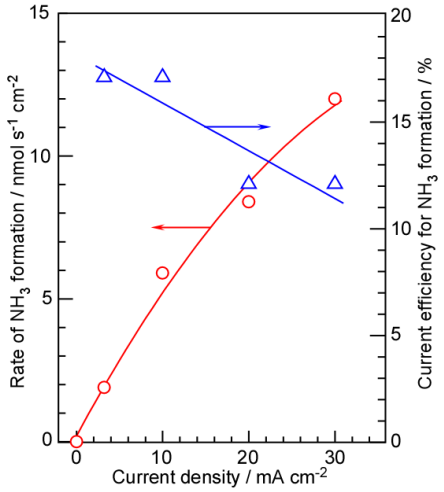

Fig. 9 Rate of NH_3 formation with increasing current density at 0.7 MPa using 5 wt%-Ru/Cs^+/MgO (Cs/Ru = 1 mol). The electrochemical hydrogen-membrane reactor was operated at 250 ˚C with a cathode gas of N_2 while maintaining the H_2/N_2 ratio at 0.071, and an anode gas of Ar of 10 cm^3_{STP} min^{-1}, with H_2O of 4 μL-liquid min^{-1}.

which dictates the equilibrium electrode potentials of the cathode and anode, are equivalent to the pure electrochemical synthesis of NH_3 with direct electrochemical reduction of N_2. The total heat and change in Gibbs energy for the chemical reaction depend only on the difference in the initial and final states of the reaction, not on the pathway. In the present electrochemical hydrogen-membrane reactor, the partial pressure of H_2 for NH_3 synthesis is kept lower than that for H_2 production in water electrolysis. Thus, the theoretical cell voltage and heat release in the present electrochemical hydrogen-membrane reactor is theoretically as same as that for electrochemical NH_3 synthesis with direct electrochemical reduction of N_2. However, the difference in theoretical voltage between electrochemical NH_3 synthesis and water electrolysis is considerably small, and this difference could not be detected experimentally. This indicates that the most advantage of present electrochemical hydrogen-membrane reactor is a simple single devise for NH_3 synthesis from N_2 and H_2O which is thermally balanced.

The electrochemical hydrogen-membrane reactor provides a unique reaction field for NH_3 synthesis. Another feature of the electrochemical hydrogen-membrane reactor is a counter-current reactor in the catalyst layer. Furthermore, as discussed following paragraphs, the target of present development is NH_3 production higher than H_2 production using one pass reactor without recycling of unreacted gases. Thus, it seems that catalyst design different from the conventional NH_3 synthesis such as Haber-Bosch process is required. In facts, as shown in Fig. 7, the rate of NH_3 formation draw away from the equilibrium limit in the higher pressure region, indicating that the present catalysts do not have enough activity for the reactor.

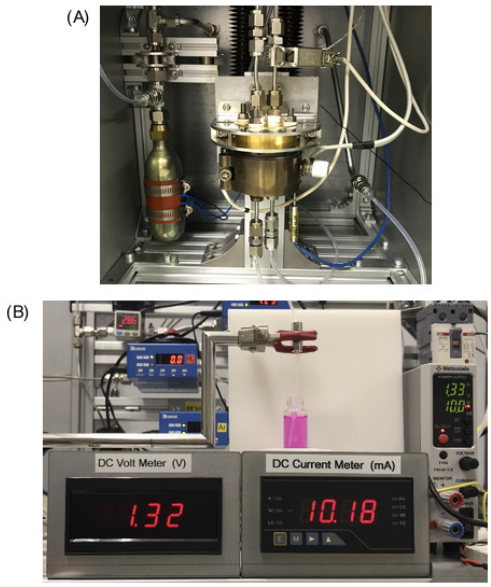

Fig. 10 Photographs of the exterior of the electrochemical hydrogen-membrane reactor (A) and bubbling of exhaust gas from the cathode side into a phenolphthalein solution (B).

In addition, since the present system had the leakage especially at high pressures, which resulted in the divergence of total current efficiency from 100% as discussed in Table 2, the sealing technique of the reactor and mechanical performance of electrolytes need to be improved.

There are essentially two reaction pathways in the present electrochemical hydrogen-membrane reactor as shown in Fig. 11. The permeated H atoms in the Pd-Ag membrane are located at the surface of the Pd-Ag membrane as adsorbed H atoms. The adsorbed H atoms are desorbed from the surface of the Pd-Ag as H_2, and then adsorbed on the Ru particles with N_2 to form NH_3 as shown in (a) in Fig. 11. Another pathway is that adsorbed H atoms spill over onto the support surfaces to reach the Ru surfaces as shown in (b) in Fig. 11. Although both pathways were possible in our previous reactor,[35,36] the spill-over pathway is less likely in the present reactor because the sintered metal powder plate between the Ru catalysts and the Pd-Ag foil prevented contact between them. If the spill-over pathway is artificially fabricated with a catalyst layer design with appropriate surface properties, the present electrochemical hydrogen-membrane reactor represents a novel reaction system. In this mechanism, selectivity for the desorption rates of NH_3 against that of H_2 can be controlled by the reaction rate kinetics but are not limited by the thermodynamic equilibrium. This is regarded as a fundamental challenge and aspiration in the future development of the present electrochemical hydrogen-membrane reactor.

The theoretical thermodynamic equilibrium of N_2, H_2, and NH_3 was calculated as shown in Fig. 12, where the equilibria at temperatures between 200 and 250°C and pressure up to 1 MPa are plotted. The thermodynamic parameters used in this calculation are shown in ESI. At 200°C and 1 MPa, the formation of 60% of NH_3 and 40% of H_2 was theoretically expected from the thermodynamics. This value was considered to be the target for further development of the present electrochemical hydrogen-membrane reactor on a laboratory

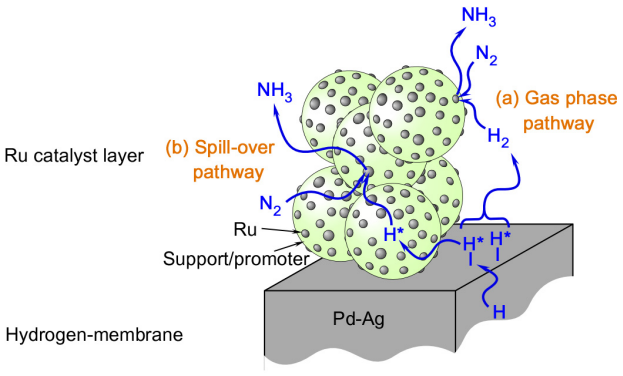

Fig. 11 Reaction mechanisms of NH_3 synthesis in the present electrochemical hydrogen-membrane reactor. Pathway (a) is the more likely mechanism, while the creation of pathway (b) is the object of further investigations.

scale. For practical utilization, 90% or higher formation of NH_3 is required, and it is reasonably considered that a pressure higher than 1 MPa is needed for practical synthesis of NH_3. Currently, electrolysis of water has reached a H_2 pressure as high as 35 MPa or more,[54,55] and it is does not seem impossible to achieve higher pressure operation for electrolysis. To improve the present electrochemical hydrogen-membrane reactor, development of active catalyst materials that operate under conditions close to equilibrium, along with optimization of the structure of the catalyst layer with counter-current flow of N_2 and H_2, are key issues.

Another challenge is the development of electrolytes. Only phosphate-based electrolytes such as CsH_2PO_4/SiP_2O_7 are useful as solid electrolytes in the temperature range of 200-250°C. However, the mechanical strength of these electrolytes is clearly poorer than that for solid oxide and polymer electrolytes. The stability of the electrochemical cell strongly depended on the quality of CsH_2PO_4/SiP_2O_7 in our experiments and the survey of stable and rigid electrolytes at 200-250°C is an important issue.

In this work, we have achieved operation at 0.7 MPa, 250°C, and 30 mA cm^{-2}, and obtained a NH_3 formation rate of 12 nmol s^{-1} cm^{-2} and a current efficiency of 12%. The attainment of equilibrium was 41% at this condition. These values were remarkably improved from our previous papers;[36] however, more improvement might be required for the practical operation of the present electrochemical hydrogen-membrane reactor.

Characterization of catalysts

As discussed above, the activity of the catalysts was the most important key to obtaining a rate of NH_3 formation close to the thermodynamic equilibrium. A detailed study on the Ru catalysts for the electrochemical hydrogen-membrane reactor at 200-250°C will appear in a forthcoming paper. The TEM images and analysis of adsorbed N_2 on Ru sites by infrared spectroscopy are presented briefly in this section.

TEM images of 5 wt%-Ru/Cs^+/MgO (Cs/Ru = 1 mol), 5 wt%-Ru/MgO, 5 wt%-Ru/Cs^+/CeO_2 (Cs/Ru = 1 mol), and 5 wt%-Ru/CeO_2 are shown in Fig. 13. For Ru/MgO, it is clearly seen that Ru particles with sizes of a few or several nanometres are uniformly dispersed on cubic-like MgO particles with sizes of 30-50 nm. For Ru/Cs^+/MgO, it was found that the cubic-shaped MgO particles were somewhat changed in shape and some Ru particles were aggregated to form large particles. The Cs^+ was loaded on Ru/MgO by immersing Ru/MgO into $CsNO_3$ aqueous solution and drying. This process was considered to change the shape of MgO and should be modified to produce finely dispersed Ru particles. For CeO_2-supported Ru catalysts, CeO_2 seemed to consist of about 10 nm particles. However, Ru particles could not be observed because of their similar atomic weight. It was speculated that Ru particles were supported on CeO_2 as reported in other literature.

Infrared spectra of adsorbed N_2 molecules on Ru catalysts were investigated as shown in Fig. 14. For Ru/MgO, the N≡N stretching vibration of adsorbed N_2 on the metallic Ru sites was observed at 2139 cm^{-1} with a shoulder at 2030 cm^{-1}. This spectral shape was the same as that reported in our previous work.[47,53] It should be noted that our previous work included $^{15}N_2$ isotope experiments and the assignment of this peak to the N ≡ N stretching vibration was not in doubt.[53,56] The appearance of a shoulder was considered to be due to the presence of Ru sites strongly interacting with MgO, which is an electronegative material. For Ru/CeO_2, the peak was observed at 2164 cm^{-1}, which was slightly higher than that for Ru/MgO. With the addition of Cs^+ promoters to Ru/MgO and Ru/CeO_2,

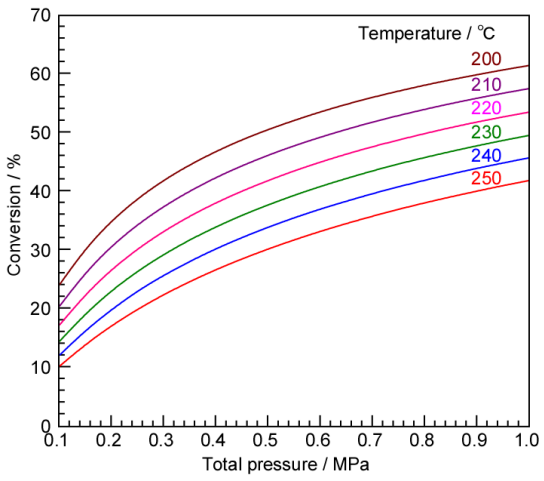

Fig. 12 Thermodynamic equilibrium of N_2 + 3 H_2 → 2 NH_3 based on conversion of H_2 in the 200-250 ˚C region.

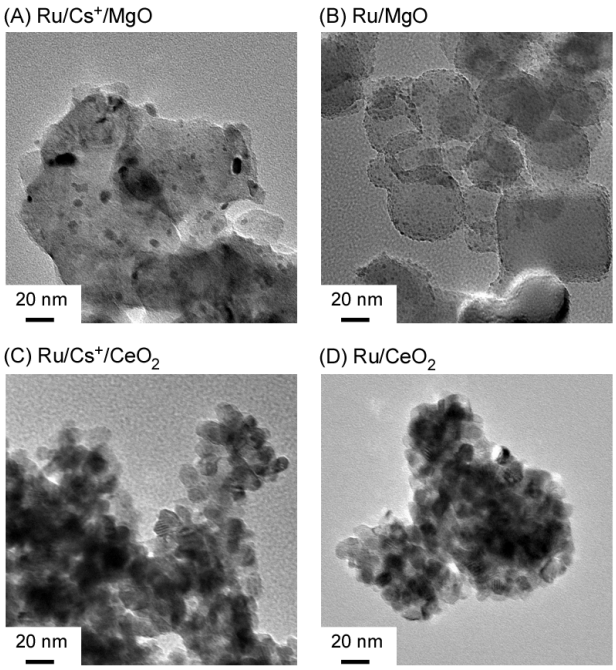

Fig. 13 TEM images of 5 wt%-Ru/Cs^+/CeO_2 (Cs/Ru = 1 mol), 5 wt%-Ru/Cs^+/MgO (Cs/Ru = 1 mol), 5 wt%-Ru/CeO_2, and 5 wt%-Ru/CeO_2.

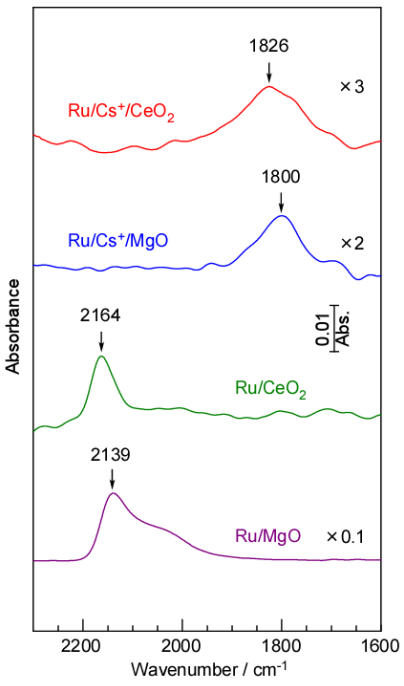

Fig. 14 Absorbance infrared spectra of adsorbed N_2 molecules on Ru sites at 15 kPa of N_2 and 30 ˚C for 5 wt%-Ru/Cs^+/MgO (Cs/Ru = 1 mol), 5 wt%-Ru/MgO, 5 wt%-Ru/Cs^+/CeO_2 (Cs/Ru = 1 mol), and 5 wt%-Ru/CeO_2. The vertical axis of each spectrum is magnified by the stated value; for example, the absorbance for the peak of adsorbed N_2 on Ru/MgO is about ten times higher than that on Ru/CeO_2. The catalysts were pretreated in 30 kPa of H_2 at 500 ˚C followed by evacuation at the same temperature in the infrared cell. N_2 gas was introduced after cooling the cell to 30 ˚C.

the frequencies of the N≡N stretching vibrations were shifted to 1800 and 1826 cm^{-1}, respectively. In our previous papers, the frequency of the N≡N stretching vibration of adsorbed N_2 molecules on Ru was found to relate to the activity for NH_3 synthesis,[47,48] because cleavage of the N≡N bond on Ru sites is the rate-determining step in NH_3 synthesis. A lower N≡N stretching vibration indicates weakening of the N≡N bond, so is preferable for N_2 dissociation. Thus, the appearance of N≡N stretching bands at 1800 and 1826 cm^{-1} indicated that the Cs^+ promoter significantly affected the Ru sites. The low-frequency shift due to the addition of Cs^+ in the present work was ca. 340 cm^{-1} in both cases of Ru/MgO and Ru/CeO_2, while ca. 260 cm^{-1} was reported in our previous work.[47,53] It has been known that electronegative promoters and supports partially donate electrons to Ru particles and anti-bonding lowest unoccupied molecular orbitals (LUMO) of N≡N π-bonds of adsorbed N_2.[56,57]

The frequencies of adsorbed N_2 on Ru for Ru/Cs^+/MgO and Ru/Cs^+/CeO_2 were quite lower than those without Cs^+, and their rates of NH_3 formation were much higher than those without Cs^+ as shown in Fig. 5. This fact follows the conclusions in our previous papers.[47,48,53] However, the frequency of adsorbed N_2 for Ru/CeO_2 was 25 cm^{-1} higher than that for Ru/MgO, although Ru/CeO_2 had a much higher rate of NH_3 formation than Ru/MgO as shown in Fig. 5. This result contradicts our previous papers.[47,48,53] It was speculated that a small amount of undetectable adsorbed N_2 was present on Ru/CeO_2, which might play a key role in the NH_3 synthesis. Ogura et al. reported a weak and broad absorption peak due to adsorbed N_2 molecules on Ru sites in Ru/$La_{0.5}Ce_{0.5}O_{1.75}$ with a low frequency of 1844 cm^{-1}. In the case of Ru/CeO_2, similar Ru sites may be present, but the infrared absorption measurements may have missed them in the present experiments because the level might be below the detection limits.

Conclusions

NH_3 synthesis from N_2 and H_2O by electrical power using an electrochemical hydrogen-membrane reactor at 200-250 ˚C was investigated with 5 wt%-Ru/Cs^+/MgO (Cs/Ru = 1 mol), 5 wt%-Ru/Cs^+/CeO_2 (Cs/Ru = 1 mol), and 5 wt%-Ru/CeO_2 catalysts under various pressure conditions. The maximum rate of NH_3 formation was obtained with Ru/Cs^+/MgO of 12.4 nmol s^{-1} cm^{-2} (759 μg h^{-1} cm^{-2}) at 0.7 MPa, 250°C, and 30 mA cm^{-2}. From the dependence of the rate of NH_3 formation on the flow rate of N_2, the rate of NH_3 formation was found to be limited by hydrogen poisoning. Thus, the optimum flow rate of N_2 was far from stoichiometry. Elevating the pressure enhanced the rate of NH_3 formation especially on Ru/Cs^+/MgO.

Conflicts of interest

There are no conflicts to declare.

Acknowledgements

This work was supported by one of the projects in “Creation of Innovative Core Technology for Manufacture and Use of Energy Carriers from Renewable Energy” of the CREST program of the Japan Science and Technology Agency (JST).

References

1 M. Boudellal, *Power-to-gas: Renewable Hydrogen Economy for the Energy Transition*, De Gruyter, Berlin, 2018.
2 D.A.J. Rand and R.M. Dell, *Hydrogen Energy: Challenges and Prospects*, Royal Society of Chemistry, London, 2007.
3 J.W. Tester, E.M. Drake, M.J. Driscoll, M.W. Golay and W.A. Peters, *Sustainable Energy: Choosing Among Options*, The MIT Press, Cambridge, MA, USA, 2012.
4 The Japan Times, https://www.japantimes.co.jp/news/2018/10/13/business/fearing-blackouts-kyushu-electric-ask-solar-power-generators-suspend-generation-saturday/#.XAjJYelRfct
5 A. Ozaki and K. Aika, *Catalysis-Science and Technology*, ed. J.R. Anderson and M. Boudart, Springer-Verlag KG, Berlin,1981, vol. 1, pp. 87–158.
6 *Ammonia: Catalysis and Manufacture*, ed. A. Nielsen, Springer-Verlag, Berlin Heidelberg, 1995.

7 H. Liu, *Ammonia Synthesis Catalysts: Innovation and Practice*, World Scientific, Singapore, 2013.
8 R.F. Service, *Science*, 2018, **361**, 120-123.
9 S. Giddey, S.P.S. Badwal, C. Munnings and M. Dolan, A. Valera-Medina, H. Xiao, M. Owen-Jones, W.I.F. David and P.J. Bowen, *Prog. Energy Combust. Sci.*, 2018, **69**, 63-102.
10 G.-F. Chen, S. Ren, L. Zhang, H. Cheng, Y. Luo, K. Zhu, L.-X. Ding and H. Wang, *Small Methods*, 2018, 1800337.
11 R. Lan, J.T.S. Irvine, S. Tao, *Int. J. Hydrogen Energy*, 2012, 37, 1482-1494.
12 S. Giddey, S. P. S. Badwal, C. Munnings and M. Dolan, *ACS Sustain. Chem. Eng.*, 2017, 5, 10231–10239.
13 C. Zamfirescu and I. Dincer, *J. Power Sources* 2008, **185**, 459.
14 A. Valera-Medina, S. Morris, J. Runyon, D.G. Pugh, R. Marsh, P. Beasley and T. Hughes, *Energy Procedia*, 2015, **75**, 118-123.
15 AIST press release, https://www.aist.go.jp/aist_e/list/latest_research/2016/20160412/en20160412.html
16 A.J. Reiter and S.-C. Kong, *Fuel*, 2011, **90**, 87-97.
17 S. Frigo and R. Gentili, *Int. J. Hydrogen Energy*, 2013, **38**, 1607-1615.
18 A. Afif, N. Radenahmad, Q. Cheok, S. Shams, J.H. Kim and A.K. Azad, *Renew. Sustain. Energy Rev.*, 2016, **60**, 822-835.
19 M. Ni, M.K.H. Leung and D.Y.C. Leung, *Int. J. Energy Res.*, 2009, **33**, 943-959.
20 T. Okanishi, K. Okura, A. Srifa, H. Muroyama, T. Matsui, M. Kishimoto, M. Saito, H. Iwai, H. Yoshida, M. Saito, T. Koide, H. Iwai, S. Suzuki, Y. Takahashi, T. Horiuchi, H. Yamasaki, S. Matsumoto, S. Yumoto, H. Kubo, J. Kawahara, A. Okabe, Y. Kikkawa, T. Isomura and K. Eguchi, *Fuel Cells*, 2017, **17**, 383-390.
21 A.F.S. Molouk, J. Yang, T. Okanishi, H. Muroyama, T. Matsui and K. Eguchi, *J. Power Sources,* 2016, **305**, 72-79.
22 USGS Nitrogen Statistics and Information, https://minerals.usgs.gov/minerals/pubs/commodity/nitrogen/mcs-2018-nitro.pdf
23 Food and Agriculture Organization of the United Nation (FAO), *World fertilizer trends and outlook to 2018.*
24 K. Matsuoka, K. Miyoshi and Y. Sato, *J. Power Sorces*, 2017, 343, 156-160.
25 J. Ikäheimo, J. Kiviluoma, R. Weiss, H. Holttinen, *Int. J. Hydrogen Energy*, 2018, **43**, 17295-17308.
26 Edit. J.R. Rumble, *CRC Handbook of Chemistry and Physics 99th*, CRC Press, Boca Raton, 2018.
27 O. A. Hougen, K. M. Watson and R. A. Ragatz, *Chemical Process Principles, Part II*, John Wiley & Sons, New York, 2nd edn, 1959.
28 Y. Ito, T. Nishikiori and H. Tsujimura, *Faraday Discuss.*, 2016, **190**, 307-326.
29 I.A. Amar, R. Lan, C.T.G. Petit and S. Tao, *J Solid State Electrochem.*, 2011, **15**, 1845-1860.
30 S. Giddey, S. P. S. Badwal and A. Kulkarni, *Int. J. Hydrogen Energy*, 2013, 38, 14576-14594.
31 A.Q. Fenwick, J.M. Gregoire, O.R. Luca, *J. Photochem. Photobio. B*, 2015, **152**, 47-57.
32 X. Guo, Y. Zhu and T. Ma, *J. Energy Chem.*, 2017, **26**, 1107.
33 L.F. Greenlee, J.N. Renner and S.L. Foster, *ACS Catal.*, 2018, **8**, 7820-7827.
34 A.J. Martín, T. Shinagawa, J. Pérez-Ramírez, *Chem*., 2019, in press.
35 K. Imamura, M. Matsuyama and J. Kubota, *Chemistry Select*, 2017, **2**, 11100-11103.
36 K Imamura and J Kubota, *Sustain. Energy Fuels,* 2018, **2**, 1278-1286.
37 Y.-H. Xie, J.-D. Wang, R.-Q. Liu, X.-.Su, Z.-P. Sun and Z.-J. Li, *Solid State Ionics*, 2004, **168**, 117-121.
38 E. Vasileiou, V. Kyriakou, I. Garagounis, A. Vourros, A.Manerbino, W.G. Coors and M. Stoukides, *Solid State Ionics*, 2016, **288**, 357–362.
39 N. Shimoda, Y. Kimura, Y. Kobayashi, J. Kubota and S. Satokawa, *Int. J. Hydrogen Energy*, 2017, **42**, 29745-29755.
40 F. Kosaka, T. Nakamura and J. Otomo, *J. Electrochem. Soc.*, 2017, **164**, F1323-F1330.
41 S. Kishira, G. Qing, S. Suzu, R. Kikuchi, A. Takagaki and S.T. Oyama, *Int. J. Hydrogen Energy*, 2017, **42**, 26843-26854.
42 S. Chen, S. Perathoner, C. Ampelli, C. Mebrahtu, D. Su and Gabriele Centi, *ACS Sustain. Chem. Enginner.*, 2017, **5**, 7393-7400.
43 Y. Aoki, S. Kobayashi, T. Yamaguchi, E. Tsuji, H. Habazaki, K. Yashiro, T. Kawada and T. Ohtsuka, *J. Phys. Chem. C*, 2016, 120, 15976–15985.
44 N. Ito, M. Iijima, K. Kimura and S. Iguchi, *J. Power Sources,* 2005, 152, 200–203.
45 N. Ito, S. Aoyama, T. Masui, S. Matsumoto, H. Matsumoto and T. Ishihara, *J. Power Sources*, 2008, **185**, 922–926.
46 S. Yamaguchi, S. Yamamoto, T. Shishido, M. Omori, A. Okubo, *J. Power Sources*, 2004, **129**, 4-6.
47 K. Aika, *Catal. Today*, 2017, **286**, 14-20.
48 K. Aika, J. Kubota, Y. Kadowaki, Y. Niwa and Y. Izumi, *Appl. Surf. Sci.*, 1997, **121/122**, 488-491.
49 Y. Ogura, K. Sato, S. Miyahara, Y. Kawano, T. Toriyama, T. Yamamoto, S. Matsumura, S. Hosokawa and K. Nagaoka, *Chem. Sci.*, 2018, **9**, 2230-2237.
50 K. Sato, K. Imamura, Y. Kawano, S. Miyahara, T. Yamamoto, S. Matsumura and K. Nagaoka, *Chem. Sci.*, 2017, 8,674-679.
51 M. Hara, M. Kitano and H. Hosono, *ACS Catal.*, 2017, **7**, 2313-2324.
52 M. Kitano, Y. Inoue1, Y. Yamazaki, F. Hayashi, S. Kanbara, S. Matsuishi, T. Yokoyama, S.-W. Kim, M. Hara and Hideo Hosono, Nature Chem., 2012, 4, 934-940.
53 J. Kubota and K. Aika, *J. Phys. Chem.*, 1994, **98**, 11293-11300.
54 A. Buttler and H. Spliethoff, *Renew. Sustain. Energy Rev.*, 2018, **82**, 2440-2454.
55 K. Onda, T. Kyakuno, K. Hattori and K. Ito, *J. Power Sources*, 2004, **132**, 64-70.
56 E.A. Wovchko and J.T. Yates, Jr, *J. Am. Chem. Soc.*, 1996, **118**, 10250-10256.
57 C.N.R. Rao and G.R. Rao, *Surf. Sci. Rep.*, 1991, **13**, 221-263.

Sustainable Energy & Fuels

PAPER

Ammonia synthesis from nitrogen and water at intermediate temperatures and elevated pressures by using an electrochemical hydrogen-membrane reactor with supported Ru catalysts and phosphate electrolytes.

Kanako Imamura and Jun Kubota

A novel electrochemical hydrogen-membrane reactor system was examined to synthesize NH_3 from N_2 and H_2O by electrical power, which enables the conversion of redundant electricity to ammonia as a chemical fuel.